Reaction of Cu^+ with dimethoxyethane: Competition between association and multiple dissociation channels

Hideya Koizumi, Felician Muntean,[a] and P. B. Armentrout[b]
Department of Chemistry, University of Utah, Salt Lake City, Utah 84112

(Received 4 August 2003; accepted 7 October 2003)

The reaction of Cu^+ with dimethoxyethane (DXE) is studied using kinetic-energy dependent guided ion beam mass spectrometry. The bimolecular reaction forms an associative $Cu^+(DXE)$ complex that is long-lived and dissociates into several competitive channels: $C_4H_9O_2^+ + CuH$, $Cu^+(C_3H_6O) + CH_3OH$, back to reactants, and other minor channels. The kinetic-energy dependences of the cross sections for the three largest product channels are interpreted with several different models (including rigorous phase space theory) to yield 0 K bond energies after accounting for the effects of multiple ion–molecule collisions, internal energy of the reactant ions, Doppler broadening, and dissociation lifetimes. These values are compared with bond energies obtained from collision-induced dissociation (CID) studies of the $Cu^+(DXE)$ complex and found to be self-consistent. Although all models provide reasonable thermochemistry, phase space theory reproduces the details of the cross sections most accurately. We also examine the dynamics of this reaction using time-of-flight methods and a retarding potential analysis. This provides additional insight into the unimolecular decay of the long-lived $Cu^+(DXE)$ association complex. Comparison of results from this study with those from the complementary CID study, thus forming the same energized $Cu^+(DXE)$ complex in two distinct ways, allows an assessment of the models used to interpret CID thresholds. © *2004 American Institute of Physics.* [DOI: 10.1063/1.1630030]

I. INTRODUCTION

In recent work, we measured the binding energies of Cu^+ with one to four dimethylether (DME)[1] and one to two bidentate dimethoxyethane ($CH_3OCH_2CH_2OCH_3$, DXE) ligands.[2] In the collision-induced dissociation (CID) of $Cu^+(DXE)$ with Xe, the simple dissociation to $Cu^+ + DXE$ along with several competing processes, reactions (1)–(4), were observed, as reproduced in Fig. 1:

$$Cu^+(DXE) + Xe \rightarrow Cu^+ + DXE + Xe, \quad (1)$$

$$\rightarrow C_4H_9O_2^+ + CuH + Xe, \quad (2)$$

$$\rightarrow Cu^+(C_3H_6O) + CH_3OH + Xe, \quad (3)$$

$$\rightarrow C_3H_7O^+ + CH_2O + CuH + Xe. \quad (4)$$

The major channel competing with simple dissociation is the loss of CuH neutral to form $C_4H_9O_2^+$, which theoretical calculations[2] indicate has a $CH_3OCH_2CH_2OCH_2^+$ structure. Reaction (3) has the lowest onset of all reactions observed, but is a relatively minor pathway, apparently because the reaction is kinetically hindered. Reaction (4) is observed at higher energies and the behavior of its cross section indicates that this ion is formed by loss of formaldehyde from the primary $C_4H_9O_2^+$ product ion. Analysis of the kinetic-energy dependences of these cross sections yields a binding energy for $CuH–C_4H_9O_2^+$, 2.70 ± 0.08 eV, that is slightly smaller than that measured for $Cu^+–DXE$, 2.79 ± 0.07 eV. Both processes were determined to have appreciable kinetic shifts, 0.69 and 0.76 eV, respectively, which are associated with energized $Cu^+(DXE)$ complexes having lifetimes that exceed the experimental flight time near their thermodynamic thresholds. Theoretical results corroborate this relative thermochemistry although the absolute bond energies from theory exceed the experimental values by 0.2–0.3 eV.[2] The kinetically hindered $Cu^+(C_3H_6O) + CH_3OH$ channel could not be modeled very accurately such that the resulting thermochemistry was imprecise, i.e., the thermodynamic threshold was determined only as 2.0 ± 0.6 eV.

A convenient way to verify the relative thermochemistry of the competing reactions (1) and (2) is to examine reaction (5):

$$Cu^+ + DXE \rightarrow CuH + C_4H_9O_2^+. \quad (5)$$

The thermochemistry derived in our CID study predicts that this reaction is exothermic by 0.09 ± 0.11 eV, a result that we imagined could be ascertained readily by studying its kinetic energy dependence using guided ion beam tandem mass spectrometry. However, as will be seen below, Cu^+ reacts with DXE molecules primarily by association to form $Cu^+(DXE)$ complexes. Thus, the kinetic energy dependence of reaction (5) is not clearly assigned as exothermic or endothermic because this reaction competes with formation of a long-lived $Cu^+(DXE)$ association complex.

Largely driven by the observations made in the present work, we have recently developed thermokinetic methods that utilize statistical unimolecular decay theory to analyze

[a]Current address: JILA, University of Colorado, Boulder, CO 80309.
[b]Electronic mail: armentrout@chem.utah.edu

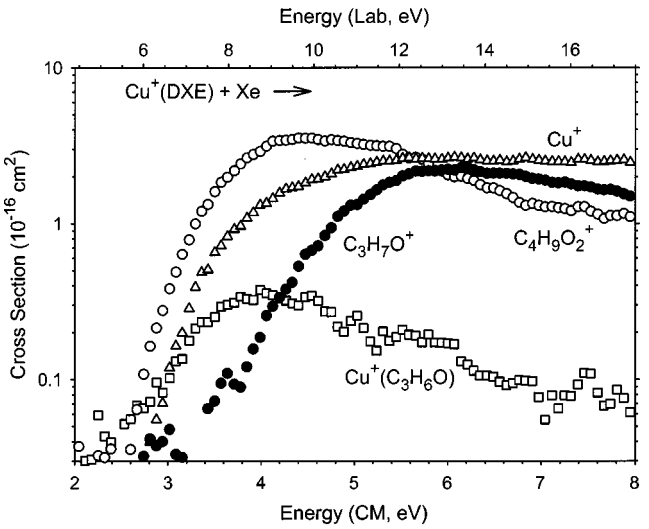

FIG. 1. Zero pressure extrapolated cross sections for the CID reactions of Cu^+(DXE) with Xe as a function of kinetic energy in the center-of-mass frame (lower x axis) and laboratory frame (upper x axis). Reproduced from Ref. 2.

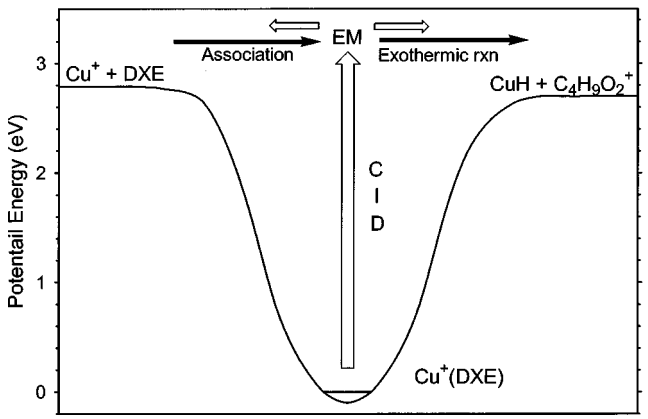

FIG. 2. Potential-energy surface for association and collision-induced dissociation (CID) reactions. Two distinct ways of forming the energized Cu^+(DXE)* molecule are shown. For CID, Cu^+(DXE)* is prepared at room temperature and collisionally excited, yielding a broad internal energy distribution and unknown angular momentum distribution. In the association reaction, Cu^+(DXE)* complexes are formed with well-characterized distributions by reacting the bare metal ion with the DXE neutral gas at room temperature.

the kinetic-energy dependence of association reaction cross sections.[3] This earlier work involves association of DXE with alkali cations (Li^+, Na^+, and K^+) where the only decay path is dissociation back to reactants. However, the association reaction of Cu^+ and DXE produces multiple products, such that the present study provides an excellent opportunity to test these newly developed methods. By comparing these results to those obtained from a self-consistent analysis of the CID data, the present study also provides an opportunity to examine assumptions regarding the use of statistical theory to describe kinetic shifts observed in CID studies. An important facet of the present work compared to the CID studies is that the bimolecular reaction of Cu^+ with DXE forms an energized Cu^+(DXE) complex with a well-defined internal energy distribution and a broad but known angular momentum distribution. In contrast, CID studies generate energized complexes with a broad range of internal energies, ranging essentially from zero to the collision energy plus the internal energy of the reactant complex, and an unknown angular momentum distribution. The relationship between association and CID reactions is illustrated in Fig. 2, which shows a schematic potential energy surface for the Cu^+(DXE) system. In addition, we find that this work provides an excellent opportunity to test the application of unimolecular theory, such as Rice–Ramsperger–Kassel–Marcus (RRKM)[4] and phase space theory[5–11] (PST) to rapidly rotating complexes. Finally, to provide more details regarding this reaction, the present study examines the dynamics of this system using time-of-flight and retarding potential methods in our recently developed double octopole system.[12]

II. EXPERIMENT

The reactions of Cu^+ with DXE are examined using a guided ion beam tandem mass spectrometer described previously.[12,13] Copper ions are produced in a dc discharge flow tube ion source.[14] At the front end of a meter long flow tube, a dc discharge in a ~10% mixture of Ar in He creates Ar^+ ions that sputter metal ions from a copper cathode. The overall gas pressure is about 0.5 Torr and typical operating conditions of the dc discharge are 1.3 kV and 30 mA. A small amount of NO gas was introduced into the flow tube to quench excited states of the Cu^+ ion, a process that eliminates excited states to less than 0.3% of the beam intensity.[15–17]

The copper ions are extracted from the source, accelerated, and focused into a magnetic sector momentum analyzer for mass analysis. The mass-selected ions are slowed to a desired kinetic energy and focused into an rf octopole ion guide.[12,18] The guide passes through a static gas cell containing the DXE gas. After exiting the gas cell, product and remaining reactant ions drift to the end of the octopole, where they are extracted and focused into a quadrupole mass filter for mass analysis. A secondary electron scintillation ion counter detects the mass-analyzed reactant and product ions. These signals are converted to absolute reaction cross sections as described previously.[13] Absolute uncertainties in these cross sections are estimated to be ±20%.

Sharp features in observed cross sections are broadened by thermal motion of the DXE gas and the distribution of ion energies. The distribution and absolute zero of the ion kinetic energies are measured using the octopole as a retarding potential analyzer.[13] The uncertainty in the absolute energy scale is ±0.05 eV (lab). Our beam distributions have a full width at half maximum (FWHM) of about 0.2 eV (lab). Kinetic energies in the laboratory frame are converted to ion energies in the center-of-mass (CM) frame by $E(\mathrm{CM}) = \mathrm{E(lab)}\ m/(M+m)$, where M and m are masses of the ion and neutral reactants, respectively. At very low energies, the conversion includes a correction for truncation of the ion beam energy distribution.[13] All energies cited are in the CM frame except as noted.

The detailed explanation of the techniques used for time-of-flight experiments and octopole retarding potential analy-

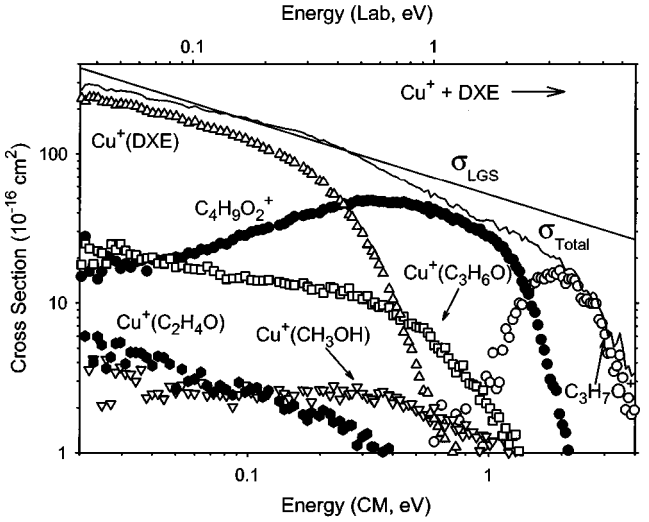

FIG. 3. Cross sections for the association reactions of Cu^+ ions with DXE as a function of kinetic energy in the center-of-mass frame (lower x axis) and laboratory frame (upper x axis). The solid lines show the total experimental cross section and the theoretical LGS cross section.

sis is given elsewhere.[12] Briefly, our instrument contains a series of two octopoles, 22.9 and 63.5 cm long, where the first octopole passes through the reaction cell. The extended length of the second octopole offers higher resolution for time-of-flight measurements. For cross-section measurements, the second octopole is typically set to float at a slightly more negative (~0.3 V) dc voltage than the first octopole to help collect slow products and to overcome local potential barriers in the long octopole. The dc voltages of these two octopoles can be controlled independently, which allows us to perform a retarding potential analysis of product ions in the second octopole, as described below.

III. RESULTS

A. Experimental cross sections

Experimental cross sections for the reaction of Cu^+ ion with DXE are shown in Fig. 3. Several products are formed as indicated in reactions (5)–(10):

$$Cu^+ + DXE \rightarrow C_4H_9O_2^+ + CuH, \quad (5)$$

$$\rightarrow C_3H_7O^+ + CH_2O + CuH, \quad (6)$$

$$\rightarrow Cu^+(CH_4O) + C_3H_6O, \quad (7)$$

$$\rightarrow Cu^+(C_2H_4O) + C_2H_6O, \quad (8)$$

$$\rightarrow Cu^+(C_3H_6O) + CH_4O, \quad (9)$$

$$\rightarrow Cu^+(DXE). \quad (10)$$

The dominant product ions observed correspond to those observed in the CID process, Fig. 1, with the addition of $Cu^+(DXE)$, the reactant in the CID study. The $Cu^+(DXE)$, $Cu^+(C_3H_6O)$, $Cu^+(C_2H_4O)$, and $Cu^+(CH_4O)$ product ions exhibit cross sections that decline with increasing energy, consistent with exothermic processes. The $Cu^+(CH_4O)$ and $Cu^+(C_2H_4O)$ product cross sections are fairly small, consistent with not observing these ions in the CID of $Cu^+(DXE)$, Fig. 1. A $C_2H_5O^+$ ion was also observed with a small cross section (<1.5 Å^2) starting near 2 eV, suggesting it is another decomposition product of $C_4H_9O_2^+$. In apparent contrast to our expectations that reaction (5) should be exothermic, the $C_4H_9O_2^+$ cross section rises with increasing energy, peaking at about 0.4 eV, before decreasing slowly up to about 1 eV. Near this energy, the cross section decreases sharply, as the $C_3H_7O^+$ cross section rises to compensate, clearly indicating that the $C_3H_7O^+$ product is formed by decomposition of $C_4H_9O_2^+$, just as in the CID studies. At low energies, the total cross section follows the predictions of the Langevin–Gioumousis–Stevenson (LGS) prediction[19] for ion–molecule collisions given a DXE polarizability (α) of 9.94 Å^3.[20] Above about 0.3 eV, the total cross section starts to deviate from the LGS prediction, behavior that we attribute to reformation of reactants, $Cu^+ + DXE$, a reaction channel that cannot be explicitly monitored.

As the formation of simple adducts is unusual in our instrument, the cross-section results were examined carefully for effects resulting from multiple collisions with the neutral DXE reagent. In particular, it is important to establish the cross section for formation of the $Cu^+(DXE)$ adduct under single collision conditions, i.e., without contributions from collisional stabilization.[3] Cross-section data was acquired originally at relatively low pressures, ~0.025 and 0.05 mTorr of DXE. The results shown in Fig. 3 have been extrapolated to zero pressure of the DXE reactant, and therefore, correspond to rigorously single collision conditions.

B. Thermochemical analysis of the associative reaction

We have modeled the three major product cross sections, reactions (5), (9), and (10), in four different ways. In all models, calculation of the unimolecular decay rate constant for $Cu^+(DXE)$ decomposing to $C_4H_9O_2^+ + CuH$ [reaction (5)] and back to reactants treats these two transition states as orbiting transition states (OTS) in the phase space limit (PSL), using equations originally developed to describe CID.[21] Previous work in our laboratory has shown that the use of this PSL is appropriate and accurate for a reaction such as the dissociation to $Cu^+ + DXE$,[21–25] and avoids the necessity of calculating molecular parameters for this pathway. The use of the PSL for reaction (5) is less obvious, but the results below indicate that this assumption is warranted, especially given the sensitivity of this system to the transition state assumptions. In all models, the rate constant for reaction (9,) is calculated using a tight transition state (TTS) for reasons described below.

The OTSs are treated variationally in that the position of the OTS depends on the angular momentum or rotational energy of the complex with a distribution that depends on the initial kinetic energy of the reactants.[3] The four models used here differ only in what assumptions are made regarding the angular momentum distribution of the complexes. Detailed explanations of these models are provided elsewhere.[3] Our "statistical model" makes a similar assumption to that used to model CID reactions,[21] namely it assumes a statistical distribution of the energy in the rotations of the complex

and further treats the two-dimensional (2D) rotor (the external rotation around the axes perpendicular to the reaction coordinate) as adiabatic but with centrifugal effects included consistent with the discussion of Waage and Rabinovitch.[26] However, this assumption fails to conserve angular momentum. To give an extreme example, a variant of the statistical model uses a delta function at $J=0$ for the distribution of the angular momentum in the adiabatic 2D rotor of the complex. This "$J=0$ model" assumes there is no external rotation involved in the dissociation along all pathways. The "$L=J$" model conserves the orbital angular momentum explicitly. No coupling between orbital and rotational angular momentum of the reactants or products is considered in this model and the rotational energy of the products is considered to be statistically distributed. The fourth model is phase space theory (PST), the rigorous statistical theory that conserves angular momentum and allows coupling between rotational and orbital motion. This should be the ideal way to calculate the rate constants. However, the PST approach sometimes breaks down when complex formation involves formation of several bonds, molecular rearrangements, steric interactions, or situations in which hard-sphere interactions are important within the range of the phase space transition state.[27]

In the statistical model, the association complex and product cross sections are modeled using Eqs. (11) and (12):

$$\sigma_{ass}(E)=\sigma_{LGS}\sum_i g_i\int_0^{J_{max}} f(J)\exp[-k_{Tot}(E^*,J)\tau]dJ, \tag{11}$$

$$\sigma_x(E)=\sigma_{LGS}\sum_i g_i\int_0^{J_{max}} f(J)\frac{k_x(E^*-E_{0x},J)}{k_{Tot}(E^*,J)} \times\{1-\exp[-k_{Tot}(E^*,J)\tau]\}dJ. \tag{12}$$

Here, σ_{LGS} is the Langevin–Gioumousis–Stevenson (LGS) collision capture cross section (as defined further below), E^* is the available energy defined as $E^*=E+E_i+E_0$, E is the center-of-mass kinetic energy, E_i is the internal energy of the reactants, $E_0=D(Cu^+-DXE)$, and $k_{Tot}(E^*,J)$ is given by Eq. (13), where x designates the various product channels, excluding the association reaction (10):

$$k_{Tot}(E^*,J)=\sum_x k_x(E^*-E_{0x},J). \tag{13}$$

The flight time, τ, used can be either the energy-dependent flight time described elsewhere[28] or an average fixed flight time (1×10^{-3} s for the systems investigated here). The average flight time is larger than the value usually cited for our double octopole apparatus[12] (5×10^{-4} s) because association reactions occur primarily at lower kinetic energies than typical CID systems and the higher mass of the association complex slows its velocity compared to the reactant ion. Indeed, we have directly measured a time of flight of about 1 ms for the Cu^+(DXE) complex as described below. The sum in Eqs. (11) and (12) is over the rovibrational states of the reactant neutral, having energies E_i and populations g_i (where $\Sigma g_i=1$). The Beyer–Swinehart algorithm is used to calculate the distribution of internal states of the DXE reactant at 305 K, the temperature of the gas in the reaction cell.[29–32] $f(J)$ is the normalized statistical distribution of the rotational angular momentum quantum number J and is given by Eq. (14)

$$f(J)=(2J+1)\rho(E^*-E_R(J))/\sum_{J=0}^{J_{max}}(2J+1) \times\rho(E^*-E_R(J)), \tag{14}$$

where J_{max} is the maximum rotational quantum number as limited by the energy available.[21] By setting $f(J)=\delta(J=0)$, we obtain an extreme model case where dissociation along all pathways does not involve any centrifugal barrier ($J=0$ model).

For the $L=J$ model, the association complex and product cross sections are calculated using Eqs. (15) and (16):

$$\sigma_{ass}(E)=\frac{\pi\hbar^2}{2E\mu}\sum_i g_i\int_0^{J_{max}}(2J+1) \times\exp[-k_{Tot}(E^*,J)\tau]dJ, \tag{15}$$

$$\sigma_x(E)=\frac{\pi\hbar^2}{2E\mu}\sum_i g_i\int_0^{J_{max}}(2J+1)\frac{k_x(E^*-E_{0x},J)}{k_{Tot}(E^*,J)} \times\{1-\exp[-k_{Tot}(E^*,J)\tau]\}dJ, \tag{16}$$

where J_{max} is defined in Eq. (17).

$$J_{max}(J_{max}+1)=(2\mu^2\alpha e^2E/\pi\varepsilon_0\hbar^4)^{1/2}. \tag{17}$$

The integrations in Eqs. (15) and (16) give Eq. (18):

$$\sigma_{Tot}(E)=\sigma_{ass}(E)+\sum_x\sigma_x(E)=\frac{\pi\hbar^2}{2E\mu}J_{max}(J_{max}+1) =\pi\left(\frac{2\alpha e^2}{4\pi\varepsilon_0E}\right)^{1/2}=\sigma_{LGS}. \tag{18}$$

Effectively, this model is the same as the statistical model with $f(J)=(2J+1)/J_{max}(J_{max}+1)$ such that the rotational distribution of the complex is no longer statistical, consistent with complexes formed in a bimolecular reaction.

PST without reactant rotational coupling also uses Eqs. (15) and (16). The only differences between the $L=J$ model and PST are the calculation of the rate constants in Eqs. (15) and (16). The PST rate constants conserve angular momentum and allow coupling between product rotational and orbital angular momenta, as described in detail elsewhere.[3] Similar coupling between the rotational and orbital angular momenta of the reactants also occurs, but the rotational component is generally negligibly small compared to the orbital component. This assumption is tested explicitly below in the present system where the reactant rotational angular momentum is not negligible compared to the orbital angular momentum.

C. Analysis of the experimental cross sections

Experimental cross sections for the associative reactions are reproduced with the different models described above as shown in Fig. 4. It is important to realize that the only adjustable parameters in all three models are E_0 and E_{0x}, the bond energy of Cu^+–DXE and the 0 K thresholds for reac-

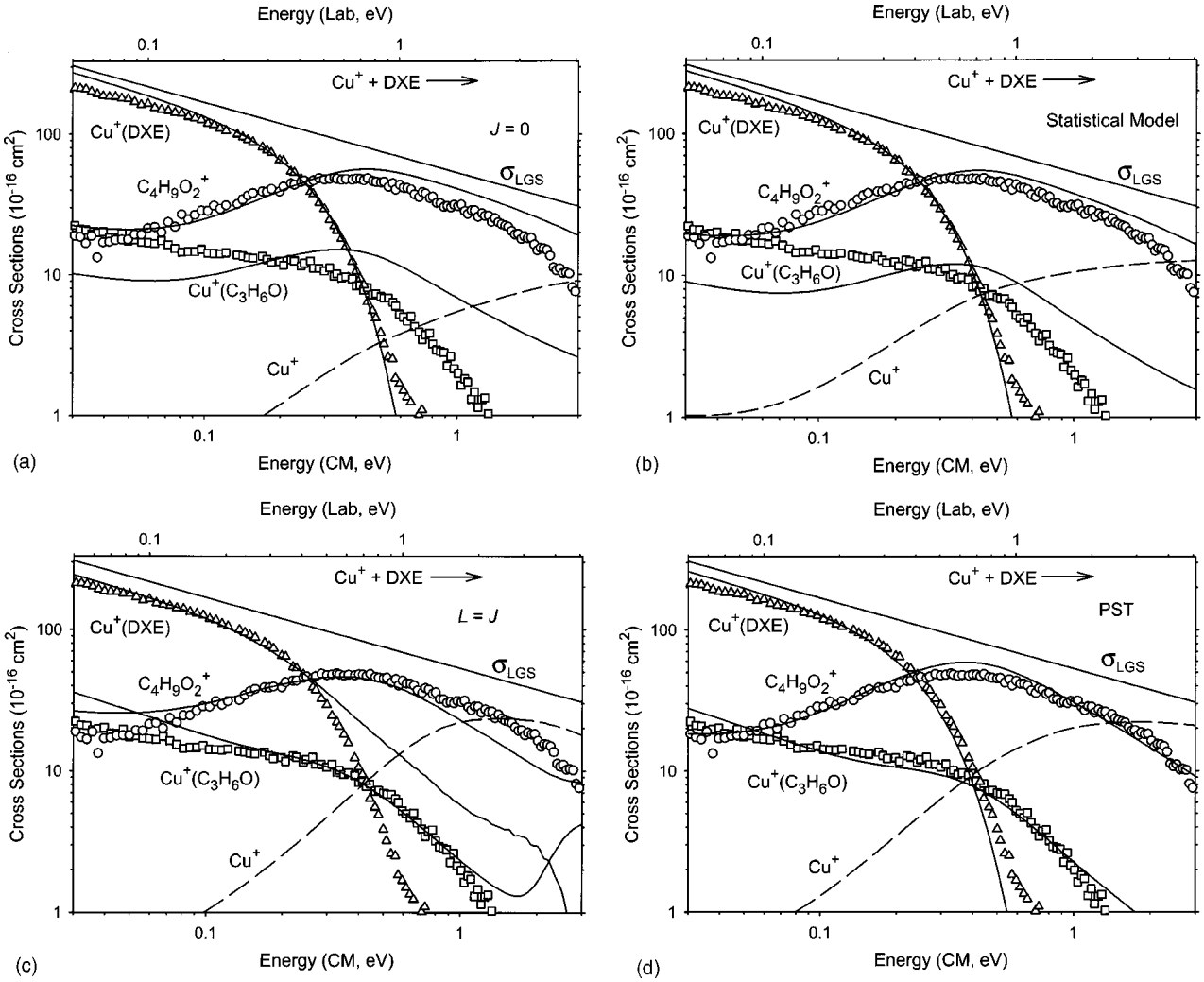

FIG. 4. Comparisons of the experimental data with models for the reaction of Cu^+ with DXE as a function of kinetic energy in the center-of-mass frame (lower x axis) and laboratory frame (upper x axis). Open squares and triangles show zero pressure extrapolated cross sections for reactions (10) and (11), respectively. Open circles are zero pressure extrapolated cross sections for reactions (5) and (6) added together. Solid lines show the best fit to the $Cu^+(DXE)$, $(C_4H_9O_2^+ + C_3H_7O^+)$, and $Cu^+(C_3H_6O)$ channel data using the bond energies listed in Table I for $J=0$ model (a), statistical model (b), $L=J$ model (c), and phase space theory (PST) (d). Dashed lines indicate the model cross sections for the $Cu^+ + DXE$ dark channel (back to reactants). The LGS cross section is also indicated.

tions (5) and (9), respectively. These control the absolute magnitudes and shapes of the predicted cross sections. The vibrational frequencies and rotational constants of DXE, $Cu^+(DXE)$, $C_4H_9O_2^+$, CuH, $Cu^+(C_3H_6O)$, and CH_3OH were calculated at the B3LYP/6-31+G* level of theory and frequencies were scaled by 0.9613.[33] These results provide all molecular constants needed for the energized complex and PSL transition states. As noted previously,[2] methanol elimination is believed to occur over a tight transition state. This was treated in two ways. One set of parameters removes a C–O stretch from the frequencies of $Cu^+(DXE)$ to represent the tighter transition state. In addition, we have performed a potential energy surface scan along the C–O stretch and located a likely tight transition state structure, shown in Fig. 5. These calculations used the B3LYP hybrid density functional method,[34,35] and a 6-31+G* basis set, and were performed using the GAUSSIAN 98 suite of programs.[36] Because this reaction involves large molecules and has a fairly complex potential energy surface, it is possible that this is not the rate limiting transition state, hence the use of both sets of parameters. Because our absolute cross sections are reported to have ±20% uncertainties in magnitude, estimates of the uncertainties in the 0 K threshold energies are obtained

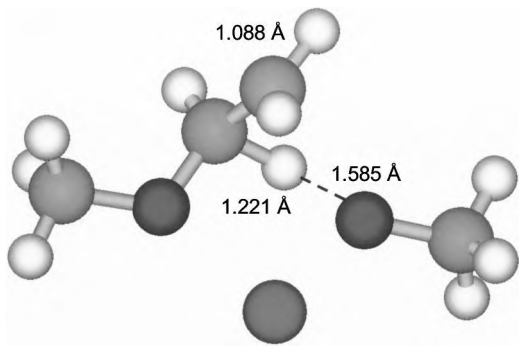

FIG. 5. The transition state structure for reaction (9) calculated at the B3LYP/6-31+G* level of theory.

TABLE I. Bond dissociation energies (eV).

Reaction	Theory[a]	CID[b]	Association		
			Statistical	$L=J$	PST
$Cu^+ + DXE$	3.08	2.79 ± 0.07	2.75 ± 0.25	2.85 ± 0.21	2.85 ± 0.23
$C_4H_9O_2^+ + CuH$	2.88	2.70 ± 0.08	2.62 ± 0.21	2.67 ± 0.18	2.69 ± 0.19
$Cu^+(C_3H_6O) + CH_3OH$	2.73[c] 1.62[d]	2.0 ± 0.6	2.30 ± 0.18	2.25 ± 0.16	2.28 ± 0.17
MAD[e] (theory)		0.24 (0.08)	0.30 (0.05)	0.22 (0.01)	0.21 (0.03)
MAD[e] (CID)	0.24 (0.08)		0.06 (0.03)	0.05 (0.02)	0.04 (0.04)

[a]B3LYP/6-31+G* level calculations including zero point energies taken from Ref. 2, except as noted.
[b]Experimental collision-induced dissociation results taken from Ref. 2.
[c]Energy of the transition state as calculated in the present work.
[d]Bond dissociation energy calculated at the product asymptote.
[e]Mean absolute deviation excluding $Cu^+(C_3H_6O) + CH_3OH$ channel.

by fitting to the experimental cross sections scaled by $\pm 20\%$, and also include variations in the time available for reaction by factors of 2 and 1/2, variations associated with uncertainties in the vibrational frequencies by $\pm 10\%$, and the error in the absolute energy scale (± 0.05 eV lab). The first quantity is by far and away the largest contributor to the absolute uncertainties reported here. The results for all models are listed in Table I along with bond dissociation energies (BDEs) from our experimental CID study and theory (B3LYP/6-31+G* level including zero-point energy corrections but no BSSE corrections).[2]

1. Statistical model

Using the statistical model, the best fits to the experimental cross sections are obtained when we set the BDEs to 2.75 ± 0.25 eV for $Cu^+ - DXE$, 2.62 ± 0.21 eV for $CuH - C_4H_9O_2^+$, and 2.30 ± 0.18 eV for $Cu^+(C_3H_6O) - CH_3OH$. The resulting BDEs agree with CID experimental results reported previously. The calculated cross sections correctly predict that the Cu^+(DXE) complex is long-lived, and therefore that reaction (10) is the dominant process with a cross section close to the collision limit at low energies, Fig. 4(b). Even though reactions (5) and (9) are exothermic (by 0.13 and 0.45 eV, respectively, for this model), the formation of these products is not predicted to be appreciable until higher energies where the Cu^+(DXE) complex begins to dissociate. The cross section for $C_4H_9O_2^+$ is nicely reproduced by this model; however, the $Cu^+(C_3H_6O)$ cross section cannot be modeled accurately without compromising the reproduction of the other two cross sections. Note that the cross section for the thermoneutral channel returning to the $Cu^+ + DXE$ reactants is also predicted by the model.

The statistical model does slightly overestimate the experimental cross sections for $C_4H_9O_2^+$ at energies above 0.4 eV, which can be explained by the following argument. The effective potential at the centrifugal barrier for reaction (5) is given by

$$V_{\text{eff}}(r_p^*)_p = V_{\text{eff}}(r^*)\alpha\mu^2/\alpha_p\mu_p^2, \tag{19}$$

where the index p refers to properties of the product channel and unindexed quantities are properties of the $Cu^+ + DXE$ reactant channel. Because $\alpha_p(6.15\ \text{Å}^3)$ is smaller than $\alpha(9.94\ \text{Å}^3)$ and μ_p (37.2 amu) is nearly same as μ (37.1 amu) for reaction (5), the centrifugal barrier is nearly 50% larger in the exit channel of reaction (5). Note that $V_{\text{eff}}(r^*)$ has a quartic dependence[3] on the orbital angular momentum quantum number J, such that the difference between the centrifugal barrier for the product and that of the reactant increases monotonically as J increases. Consequently, reaction (5) becomes less favored while dissociation back to reactants becomes more favored as J increases. However, the cross section for reaction (5) is overestimated by the statistical model because the distribution of J is concentrated at small J. To test this, we modeled the cross sections using Eqs. (11) and (12) but replacing Eq. (14) by a delta function, $\delta(J = n \times 100)$ for $n = 0$, 1, 2, 3, and 4, with fixed values of E_0 and E_{0x}. The model cross sections for $C_4H_9O_2^+$ increase in magnitude up to $J = 200$, a centrifugal acceleration described elsewhere,[3,21] and decrease significantly at higher J.[3] Such calculations for the $J = 0$ model are shown in Fig. 4(a). Note that this $J = 0$ model also overestimates the branching ratio for reaction (5) at energies above 0.4 eV, consistent with the explanation given here.

We could not find a good fit using the statistical model for reaction (9), $Cu^+(C_3H_6O) + CH_3OH$, whether an orbiting or tight transition state was used. When an orbiting transition state was used for reaction (9), we could not find any parameters that gave a cross section that declined with energy having a magnitude similar to that of the experimental cross sections. This relates to the number of rotations in the OTS for each channel [5, 6, and 3 fragment rotations for reactions (5), (9), and back to reactants, respectively]. Because reaction (9) has the maximum number of rotations in its OTS, the rate constant for this channel increases faster than the other two channels with respect to energy. As a consequence, the model cross section for reaction (9) is found to increase with energy, in contrast to the experimental behavior. Therefore, an OTS is inappropriate for reaction (9), not only for the statistical model, but for the $L = J$ model and PST as well. Two sets of TTS parameters, described above, were tested for reaction (9). Both of these model cross sections show similar characteristics in which the magnitude is correctly described but the energy dependence is inaccurate. Both increase up to 0.4 eV and gradually decrease at higher energy. However, the model cross sections for reaction (9) decrease more slowly than the experimental cross sections,

with the discrepancy being worse for the molecular parameters derived from *ab initio* calculations. This is because the rotational constant for the calculated TTS is smaller than that estimated from the $Cu^+(DXE)$ complex and a smaller rotational constant leads to a larger density of states and a larger rate constant for decomposition to this channel.[3] The resulting BDE obtained using molecular parameters derived from *ab initio* calculations is about 0.1 eV higher than the BDE found using the other set of molecular parameters (as listed in Table I) in all models. However, this difference is smaller than the absolute uncertainty in the threshold determination for any of the models (0.16–0.18 eV).

The BDE for reaction (9), 2.30 ± 0.18 eV, is higher than the theoretical BDE (1.62 eV) calculated at $Cu^+(C_3H_6O) + CH_3OH$ dissociation limit. This discrepancy arises because this reaction occurs over a barrier corresponding to a tight transition state. Calculations of this transition state at the B3LYP/6-31+G* level of theory including zero-point energies predict that it lies 2.73 eV above $Cu^+(DXE)$. This energy is 0.35 eV below the calculated $Cu^+ + DXE$ asymptote, in reasonable agreement with the experimental difference of 0.45 eV, Table I.

2. L=J model

Using the $L=J$ model, the best fits to the experimental cross sections are obtained when we set the BDEs to 2.85 ± 0.21 eV for Cu^+-DXE, 2.67 ± 0.18 eV for $CuH-C_4H_9O_2^+$, and 2.25 ± 0.16 eV for $Cu^+(C_3H_6O) - CH_3OH$. These BDEs are in good agreement with the CID experimental results reported previously,[2] Table I. The model cross sections, where the estimated TTS is used for reaction (9), are shown in Fig. 4(c). Now, the reproduction of all three channels is reasonable at low energies but the model for the association cross section greatly exceeds the experimental cross section at higher energy and those predicted for the two dissociation channels show nonmonotonic behavior [most obvious in the $Cu^+(C_3H_6O)$ cross section] at high energies. The large values of J (high centrifugal barrier for dissociation) are responsible for these deviations as described in detail elsewhere.[3] The $L=J$ model cross section for $C_4H_9O_2^+$ underestimates the experimental cross section at moderate energies (>0.4 eV). This is the opposite effect observed in the statistical model. To see why this is so, note that J_{max} is the most probable value of J in the $L=J$ model because the J distribution, $(2J+1)$, is a linearly increasing function. Again, the centrifugal barrier is larger for reaction (5) than for the return to reactants, Eq. (19), such that reaction (5) cannot conserve angular momentum for large J values. Therefore, the $L=J$ model cross section for reaction (5) is smaller than that of the statistical model, and conversely the cross section for $Cu^+ + DXE$ [dashed lines in Figs. 4(b) and 4(c)] is larger in the $L=J$ model than in the statistical model.

The model cross section for reaction (9) decreases monotonically with energy (until very high energies) in contrast to the statistical model. This can be explained by the following argument. Unlike the statistical model, the probability of getting a particular value of J steadily decreases with increasing energy ($E^{-1/2}$ dependence) because the distribution is a linearly increasing function and J_{max} increases as the energy increases. In addition, the absolute magnitude of the product cross section for reaction (9) decreases monotonically as J increases because the barrier height increases as a result of increasing rotational energy and because there is no centrifugal acceleration, in contrast to the other major competing channels that decompose over orbiting transition states. As the energy increases, the $2J+1$ distribution weights larger J values such that the cross section magnitude becomes monotonically decreasing. The resulting barrier for reaction (9) determined by using the $L=J$ model is 0.60 eV lower than the $Cu^+ + DXE$ asymptote, somewhat larger than the theoretically predicted difference of 0.35 eV, Table I.

3. Phase space theory

For phase space theory, the optimum BDEs are 2.85 ± 0.23, 2.69 ± 0.19, and 2.28 ± 0.17 eV for Cu^+-DXE, $CuH-C_4H_9O_2^+$, and $Cu^+(C_3H_6O)-CH_3OH$, respectively. The model cross sections, with the first two channels treated as having orbiting (PSL) transition states and reaction (9) treated using the estimated TTS, are shown in Fig. 4(d). It can be seen that the reproduction of the data throughout the entire energy range studied is excellent with the only adjustable parameters, the BDEs, in good agreement with the CID experimental results reported previously.[2] The strong deviations between predictions and experimental results found for the $L=J$ model are not observed in any of the PST cross sections. This is because PST allows coupling between orbiting angular momentum and rotational angular momentum whereas the $L=J$ model does not allow such coupling. Such coupling statistically favors lowering the centrifugal barrier for trajectories with large J.[3] Therefore, the PST rate constant is larger than the $L=J$ model rate constant for large J. The PST model reproduces the experimental cross sections nicely in both magnitude and shape for all channels at all energies, Fig. 4(d). The PST cross section for reaction (5) fits the experimental cross section at high energy even though PST uses the same J distribution as the $L=J$ model, which underestimates the experimental cross section. The PST cross section for reaction (5) increases at large J compared to that of the $L=J$ model because coupling of rotational and orbital angular momenta allows a lower centrifugal barrier.[3]

The cross section for reaction (9) declines monotonically with energy for the same reason as in the $L=J$ model. The PST model cross sections fit the experimental cross section nicely at all energies. The barrier determined for reaction (9) is lower than the $Cu^+ + DXE$ asymptote by 0.57 eV, comparable to the difference determined with the $L=J$ model, and somewhat larger than the theoretical difference of 0.35 eV, Table I.

We also performed calculations where the orbital and rotational angular momenta of the *reactants* were allowed to couple to yield the angular momentum in the EM.[3] This more rigorous treatment gave an identical result to that shown here. For this system, this is not because the reactant rotational angular momentum is small (average value is about 40 $\hbar$) but because the coupling with the orbital angular

momentum can both increase and decrease the angular momentum of the energized molecule. Thus, the average remains nearly constant.

D. Time of flight analysis

In order to determine the axial velocity distribution of ions, the guided ion beam instrument is operated in the *time-of-flight* (TOF) mode using the octopole ion guides as a free flight sector. A calibration procedure is needed in order to be able to convert the measured TOF distribution into an axial velocity distribution.[12] This procedure works well for transforming the data for the $Cu^+(DXE)$ association complex. However, because the $Cu^+(DXE)$ association complex is long lived, $C_4H_9O_2^+$ and $Cu^+(C_3H_6O)$ product formation occurs in both the first and second octopole where the voltages differ slightly for the reason described above. As a consequence, $C_4H_9O_2^+$ and $Cu^+(C_3H_6O)$ product velocity distributions cannot be given by a simple transformation because the resultant velocity distribution depends on where the reaction occurs. For example, a product formed in the first octopole has a larger velocity in the second octopole than a product formed in the second octopole because the dc voltage offset between the two octopoles increases the velocity of a product formed in the first octopole (lighter mass at the entrance of the second octopole) more than that of a product formed in the second octopole (mass of the energized molecule at the entrance of the second octopole). However, a model TOF distribution can easily be generated from trial velocity distributions of products formed in each octopole if the proportion of products formed in each octopole is known. Fortunately, these proportions are easily calculated from the unimolecular dissociation rate constants established above.

Trial axial product velocity distributions are converted into TOF distributions using

$$t_p = t_0\sqrt{q_r m_p/q_p M} + l_p/v_p + l_2/\sqrt{v_p^2 + 2q_p\Delta V/m_{p*}} + (l_1 - l_p)/\langle v_r\rangle, \quad (20)$$

where l_1 and l_2 are the length of the first and second octopoles, q_r is the charge of the reactant ion, M is the mass of the reactant ion, v_p is the product velocity distribution in the first octopole, V is the dc floating voltage of the first octopole, ΔV is the dc offset between the two octopoles, and $\langle\ \rangle$ brackets represent the average velocity of the reactant ion. The index p refers to product quantities and l_p is the distance from the middle of the collision cell to the end of the first octopole (11.8 cm). The quantities m_p and m_{p*} are the mass of the product ion detected and the mass of the ion at the entrance of the second octopole, respectively. Note that m_p and m_{p*} are not always the same for a reaction that involves a long-lived complex such as the association reaction studied here. The first term in Eq. (20) represents the TOF outside the octopoles, i.e., the time from the end of the second octopole to the detector. The second term is the TOF spent in the first octopole, the third term is the TOF spent in the second octopole, and the fourth term represents the TOF spent by reactant ions in the first octopole, before collision.

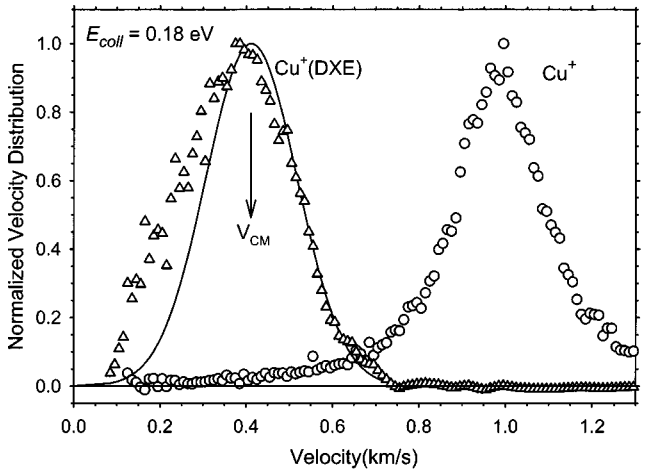

FIG. 6. Normalized velocity distributions of Cu^+ (open circles) and $Cu^+(DXE)$ (open triangles) obtained using TOF methods are shown. The arrow indicates the velocity of the center of mass, v_{CM}. The solid line is the model distribution of $Cu^+(DXE)$, Eq. (21).

E. Axial velocity distribution by TOF

The axial velocity distribution at 0.18 eV collision energy (0.31 eV lab) for the $Cu^+(DXE)$ association complex is shown in Fig. 6 along with that for the Cu^+ reactant ions. As must be the case, the $Cu^+(DXE)$ distribution is centered about the velocity of the center of the mass system. The axial velocity distribution of the complex can be derived using conservation of linear momentum and is given by Eq. (21)

$$h(v_T) = \frac{\int_{-\infty}^{\infty} f(v_i)g(v_N)dv_N}{\int_{-\infty}^{\infty}\int_{-\infty}^{\infty} f(v_i)g(v_N)dv_N dv_T}, \quad (21)$$

where $f(v_i)$ is the velocity distribution of the ion beam and $g(v_N)$ is the thermal velocity distribution of the neutral DXE target gas. The velocity of the reactant ion is $v_i = (m_T v_T - m v_N)/M$, where m_T is the mass of the association complex, m is the mass of the reactant DXE neutral, M is the mass of the reactant Cu^+ ion, v_N is the velocity of the reactant neutral, and v_T is the velocity of the association complex. The model of the velocity distribution of all transiently formed association complexes peaks at v_{cm} with a width determined by the measured reactant ion and neutral velocity distributions. This model reproduces the experimental velocity distribution of the $Cu^+(DXE)$ complex quite nicely, Fig. 6. The velocity distribution shows a tail in the low velocity region, which is caused by multiple collisions between ions and neutral reactants, as observed previously.[12] Comparable behavior is observed at a collision energy of 0.27 eV (0.46 eV lab).

In order to obtain the model TOF distribution for the $C_4H_9O_2^+$ and $Cu^+(C_3H_6O)$ channels, trial velocity distributions are considered. Because we are dealing with a long-lived $Cu^+(DXE)$ complex that survives more than several rotational periods, the velocity distributions of products that form from unimolecular decay of the long-lived complex must be symmetric, centered around the center-of-mass velocity but broadened by the kinetic-energy release. We consider two product velocity distributions that have the form of Gaussian functions where they correspond to the product

forming in the first and second octopoles. The relative probabilities of these two distributions can be provided by the probability for product formation, given most succinctly as the ratio of $\sigma_x(E)$, Eq. (16) for PST, to $\sigma_{\mathrm{Tot}}(E)$, Eq. (18), where E is the collision energy in the center-of-mass frame. Here, τ equals the time for the complex to travel from the reaction cell to either the end of the first octopole or to the end of the second octopole. These different times change the $1-\exp[-k_{\mathrm{Tot}}(E^*,J)\tau]$ term in Eq. (16). These flight times are used to calculate the probability of product formation in the first and both octopoles, respectively, and from the difference, we can obtain the proportion of the product formation occurring in each octopole. The calculations of these probabilities use PST rate constants with parameters obtained above and the average internal energy of the reactants. We find that 32 (68) and 36 (64)% of the products observed are formed in the first (second) octopole for energies equal to 0.18 and 0.27 eV, respectively.

Given the relative probabilities of forming products in the two octopoles, we require only the width of the distribution in order to formulate a trial velocity distribution that can be transformed to a TOF distribution for comparison to the experimental TOF distributions. These widths were varied until reasonable reproduction of the data was achieved, as shown in Fig. 7 for the TOF distributions of $C_4H_9O_2^+$ and $Cu^+(C_3H_6O)$ at 0.18 eV collision energy. Good reproductions of the experimental TOF distributions are achieved for both product channels at both the 0.18 and 0.27 eV collision energies. Therefore, we conclude that both $C_4H_9O_2^+$ and $Cu^+(C_3H_6O)$ are formed by dissociation of a long-lived Cu^+(DXE) complex. The full width at half maximum (FWHM) needed to reproduce the velocity distributions of both $C_4H_9O_2^+$ and $Cu^+(C_3H_6O)$ are slightly larger (350 and 400 m/s for 0.18 and 0.27 eV, respectively) than that for the Cu^+(DXE) associative complexes (300 m/s at both energies), indicating that there is some kinetic-energy release into these product channels. These product velocity distributions include the initial spread in the velocity distribution of the complex, such that deconvolution must be used to obtain approximate axial velocity distributions of the product ions. This procedure gives FWHM of the $C_4H_9O_2^+$ product ion velocity distributions of 180 and 260 m/s at collision energies of 0.18 and 0.27 eV, respectively, and 180 m/s for the $Cu^+(C_3H_6O)$ ion product velocity distributions at both collision energies. We believe that the similarity of the product velocities for the two reactions is serendipitous as further indicated by converting these velocities to energy releases. The energy of relative translation is given by Eq. (22), where v_i is the velocity of the reactant ion.

$$E_{\mathrm{rel}}=\frac{1}{2}\left(\frac{M^2+Mm}{m}\right)v_i^2. \tag{22}$$

At a collision energy of 0.18 eV, the relative translational energy release for the product of reaction (9), 0.10 $\pm$0.08 eV, is about twice as large as that for the product of reaction (5), 0.04$\pm$0.02 eV. These relative energies are consistent with the total available energies of 0.52 and 0.93 eV for reactions (5) and (9), respectively. The percentages of energy that go into translation are 7$\pm$3 and 11$\pm$8%, respectively. At a collision energy of 0.27 eV, the relative translational energies (percentages) are 0.08$\pm$0.02 eV (13$\pm$4%) and 0.10$\pm$0.08 eV (10$\pm$8%) for reactions (5) and (9), respectively. The low percentages found seem consistent with a statistically behaved system, although one might have expected a larger kinetic-energy release for reaction (9) where the process involves going over a tight transition state.

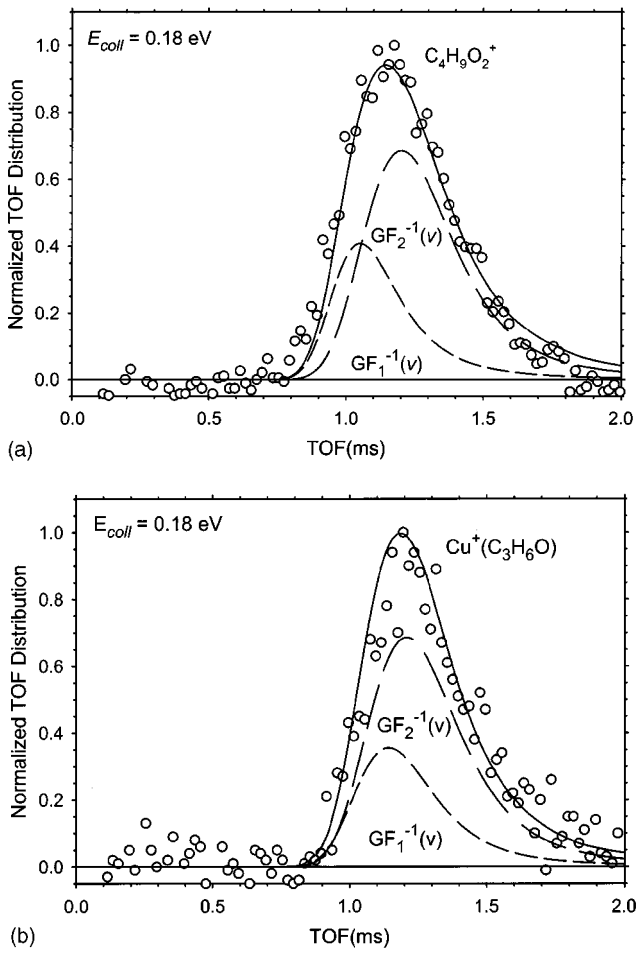

FIG. 7. Open circles represent normalized experimental TOF distributions of $C_4H_9O_2^+$ (a) and $Cu^+(C_3H_6O)$ (b). Dashed lines show the trial velocity distribution functions (Gaussian functions in velocity space) for ions formed in the first and second octopole after transformation to TOF distributions, $GF_1^{-1}(v)$ and $GF_2^{-1}(v)$, respectively. Solid lines show the sum of the two functions.

F. Retarding potential analysis

Additional insight into the dynamics of the association reaction can be obtained by a retarding potential analysis of the product ions. This is achieved by varying the potential of the second octopole relative to the first octopole at a fixed collision energy (potential of the first octopole relative to the ion source). The branching ratios of Cu^+(DXE), $C_4H_9O_2^+$, and $Cu^+(C_3H_6O)$ at a collision energy of 0.13 eV (0.22 eV lab) as a function of the relative voltage on the second octopole are shown in Fig. 8. The intensity of the $C_4H_9O_2^+$ and $Cu^+(C_3H_6O)$ products decays at higher negative voltages whereas the Cu^+(DXE) association complex intensity increases. This is because positive ions move faster as the voltage on the second octopole decreases, such that the ions

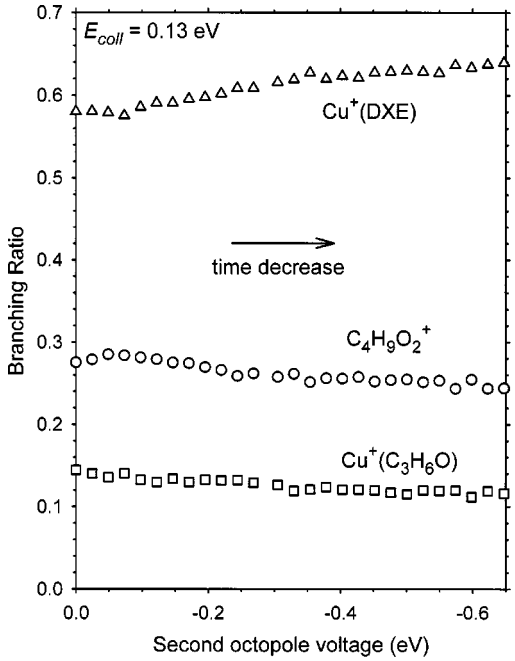

FIG. 8. Branching ratios for Cu^+(DXE) (open triangles), $C_4H_9O_2^+$ (open circles), and $Cu^+(C_3H_6O)$ (open squares) at a collision energy of 0.13 eV are shown as a function of the relative voltage on the second octopole.

arrive at the quadrupole analyzer in a shorter time, providing less time for dissociation of the association complex. Of course, this makes sense only if the products form through unimolecular decay of the association complex, additional evidence for this hypothesis.

IV. CONCLUSION

Reactions of bare Cu^+ ion and DXE neutral are studied using kinetic-energy dependent tandem mass spectrometry. The dominant reaction at low energies is formation of the Cu^+(DXE) association complex, with several competing decomposition pathways observed. We model the cross sections for the association complex and the two major decay pathways, $C_4H_9O_2^+ + CuH$ and $Cu^+(C_3H_6O) + CH_3OH$, in four different ways. In all models, calculation of the unimolecular decay rate constant treats the transition states in the phase space limit (PSL), using equations originally developed to describe the dissociation in CID,[21] except for the loss of methanol channel where a tight transition state is needed. The four models differ in how the angular momentum of the complexes is treated, but all involve careful treatments of lifetime effects, kinetic-energy distributions of the ion and neutral reactants, reactant internal energy distributions, and angular momentum distributions. With molecular parameters established by theoretical calculations, the only adjustable parameters are the relative energies of the reactants and various products. For all four models, the thermochemistry derived from reproducing the data are well within experimental error of values reported previously for collision-induced dissociation experiments, Table I. However, the best reproduction of the experimental cross sections are provided by phase space theory where the model cross sections reproduce all of the experimental cross sections in detail at all energies. The model cross sections deviate from the experimental cross sections slightly in both the statistical and $L=J$ models. This shows that the product branching ratio (but not the thermochemistry) is sensitive to the angular momentum distribution and inclusion of rotational-orbital angular momentum coupling.

An important facet of the present work compared to the CID studies is that the bimolecular reaction of Cu^+ with DXE forms an energized Cu^+(DXE) complex with a well-defined internal energy distribution and a broad but known angular momentum distribution. Because these carefully analyzed results of association reactions are in excellent agreement with those obtained from an analysis of CID data on the same systems, the present study verifies the accuracy of our assumptions regarding the use of statistical theory to describe kinetic shifts observed in CID studies.

Our recently developed TOF and double octopole system are used to study the velocity distributions of the Cu^+(DXE) association complex and $C_4H_9O_2^+$ and $Cu^+(C_3H_6O)$ product ions. The velocity distributions of all three products are centered at the velocity of the center-of-mass, showing that product formation occurs via long-lived complex formation. Transformation of the TOF distribution of the Cu^+(DXE) product to a velocity distribution is straightforward, whereas the TOF distributions for the $C_4H_9O_2^+$ and $Cu^+(C_3H_6O)$ product ions require that the effects of decomposition in both octopoles be included. Nevertheless, reproduction of these distributions is achieved with several simple assumptions. These experiments provide rough kinetic-energy release information regarding the two product ions.

ACKNOWLEDGMENTS

This work is supported by the National Science Foundation, CHE-0135517. H.K. thanks group members for enlightening discussions.

[1] H. Koizumi, X.-G. Zhang, and P. B. Armentrout, J. Phys. Chem. A **105**, 2444 (2001).
[2] H. Koizumi and P. B. Armentrout, J. Am. Soc. Mass Spectrom. **12**, 480 (2001).
[3] H. Koizumi and P. B. Armentrout, J. Chem. Phys. (to be published).
[4] R. A. Marcus and O. K. Rice, J. Phys. Colloid Chem. **55**, 894 (1951); R. A. Marcus, J. Chem. Phys. **20**, 359 (1952); H. M. Rosenstock, M. B. Wallenstein, A. L. Wahrhaftig, and H. Eyring, Proc. Natl. Acad. Sci. U.S.A. **38**, 667 (1952).
[5] P. Pechukas and J. C. Light, J. Chem. Phys. **42**, 3281 (1965); J. Lin and J. C. Light, *ibid.* **43**, 3209 (1965); J. C. Light, Discuss. Faraday Soc. **44**, 14 (1967).
[6] E. Nikitin, Teor. Éksp. Khim. 1 **135**, 144, 428 (1965).
[7] W. J. Chesnavich and M. T. Bowers, J. Chem. Phys. **66**, 2306 (1977).
[8] W. J. Chesnavich and M. T. Bowers, J. Am. Chem. Soc. **98**, 8301 (1976).
[9] C. E. Klots, J. Phys. Chem. **75**, 1526 (1971).
[10] C. E. Klots, Z. Naturforsch. A **27**, 553 (1972).
[11] D. A. Webb and W. J. Chesnavich, J. Phys. Chem. **87**, 3791 (1983).
[12] F. Muntean and P. B. Armentrout, J. Chem. Phys. **115**, 1213 (2001).
[13] K. M. Ervin and P. B. Armentrout, J. Chem. Phys. **83**, 166 (1985).
[14] R. H. Schultz, K. C. Crellin, and P. B. Armentrout, J. Am. Chem. Soc. **113**, 8590 (1991).
[15] B. L. Kickel and P. B. Armentrout, J. Phys. Chem. **99**, 2024 (1995).
[16] M. T. Rodgers, B. Walker, and P. B. Armentrout, Int. J. Mass Spectrom. Ion Processes **182/183**, 99 (1999).
[17] C. Rue, P. B. Armentrout, I. Kretzschmar, D. Schröder, and H. Schwarz, J. Phys. Chem. A **106**, 9788 (2002).
[18] S. Mark and D. Gerlich, J. Chem. Phys. **209**, 235 (1996).

[19] G. Gioumousis and D. P. Stevenson, J. Chem. Phys. **29**, 294 (1958).
[20] K. J. Miller, J. Am. Chem. Soc. **112**, 8533 (1990).
[21] M. T. Rodgers, K. M. Ervin, and P. B. Armentrout, J. Chem. Phys. **106**, 4499 (1997).
[22] M. T. Rodgers and P. B. Armentrout, J. Phys. Chem. A **101**, 1238 (1997).
[23] M. T. Rodgers and P. B. Armentrout, J. Phys. Chem. A **101**, 2614 (1997).
[24] M. T. Rodgers and P. B. Armentrout, J. Phys. Chem. A **103**, 4955 (1999).
[25] P. B. Armentrout and M. T. Rodgers, J. Phys. Chem. A **104**, 2238 (2000).
[26] E. V. Waage and B. S. Rabinovitch, Chem. Rev. **70**, 377 (1970).
[27] R. C. Dunbar, Int. J. Mass Spectrom. Ion Processes **160**, 1 (1997).
[28] F. Muntean, L. Heumann, and P. B. Armentrout, J. Chem. Phys. **116**, 5593 (2002).
[29] T. S. Beyer and D. F. Swinehart, Communications of the Association of Computing Machinery **16**, 379 (1973).
[30] S. E. Stein and B. S. Rabinovitch, J. Chem. Phys. **58**, 2438 (1973).
[31] S. E. Stein and B. S. Rabinovitch, Chem. Phys. Lett. **49**, 183 (1977).
[32] R. G. Gilbert and S. C. Smith, *Theory of Unimolecular and Recombination Reactions* (Blackwell Scientific Publications, Oxford, 1990).
[33] J. B. Foresman and A. E. Frisch, *Exploring Chemistry with Electronic Structure Methods*, 2nd ed. (Gaussian, Pittsburgh, PA, 1996).
[34] A. D. Becke, J. Chem. Phys. **98**, 5648 (1993).
[35] C. Lee, W. Yang, and R. G. Parr, Phys. Rev. B **37**, 785 (1988).
[36] M. J. Frisch, G. W. Trucks, H. B. Schlegel *et al.*, GAUSSIAN 98, Revision A.7, Gaussian, Inc., Pittsburgh PA, 1998.